REPORT

POLYMER SCIENCE

Thermal processing of diblock copolymer melts mimics metallurgy

Kyungtae Kim,[1]* Morgan W. Schulze,[1]*† Akash Arora,[1]* Ronald M. Lewis III,[1] Marc A. Hillmyer,[2] Kevin D. Dorfman,[1]‡ Frank S. Bates[1]‡

Small-angle x-ray scattering experiments conducted with compositionally asymmetric low molar mass poly(isoprene)-*b*-poly(lactide) diblock copolymers reveal an extraordinary thermal history dependence. The development of distinct periodic crystalline or aperiodic quasicrystalline states depends on how specimens are cooled from the disordered state to temperatures below the order-disorder transition temperature. Whereas direct cooling leads to the formation of documented morphologies, rapidly quenched samples that are then heated from low temperature form the hexagonal C14 and cubic C15 Laves phases commonly found in metal alloys. Self-consistent mean-field theory calculations show that these, and other associated Frank-Kasper phases, have nearly degenerate free energies, suggesting that processing history drives the material into long-lived metastable states defined by self-assembled particles with discrete populations of volumes and polyhedral shapes.

The packing and spatial arrangement of atoms and molecules determine many of the associated physical properties of condensed matter. Superficially, hard materials such as metals are deceptively simple to understand based on classical concepts modeling atoms as hard spheres that interact through pairwise attractive and repulsive forces. Cooling metals below the melting temperature leads to symmetry-breaking and the formation of crystalline states; most elemental metals form densely packed structures with body-centered cubic (bcc), face-centered cubic (fcc), or hexagonal close-packed (hcp) symmetry. However, when cooled to low temperatures, certain elemental metals, notably manganese (*1*) and plutonium (*2*), adopt a number of remarkably complex, low-symmetry crystal structures containing large unit cells with many atoms. Metal alloys offer much greater structural diversity (*3*), including aperiodic order, known as quasicrystals, characterized by rotational but not translational symmetry (*4*). A distinguishing feature of such low-symmetry crystals is the tetrahedral grouping of atoms, resulting in four types of clusters with 12-, 14-, 15-, or 16-fold coordination, as articulated by Frank and Kasper 60 years ago (*5*). Understanding the fundamental origins of symmetry selection in metals and alloys under equilibrium and nonequilibrium conditions, including the role of electronic structure, remains a central challenge in materials science and engineering (*6*).

Self-assembling soft materials—including surfactants and lipids (*7*), supramolecular assemblies (*8*–*10*), and block polymers (*11*, *12*)—are governed by seemingly very different molecular packing phenomena. Undiluted AB diblock copolymers composed of an A block bonded to a B block are perhaps the simplest archetypal case. Stitching together two linear sequences of repeat units into a single chain (Fig. 1A) results in a macromolecule that can self-organize into a variety of nanoscale morphologies that depend primarily on the composition $f_A = N_A/N$, where N_A is the normalized degree of polymerization of the A block and $N = N_A + N_B$ (*13*). In the most asymmetric variants, $f_A \ll ½$, diblock copolymers form point particles, nominally spherical in shape (Fig. 1B). When packed together in the absence of a diluent, these "soft" micelles are forced to assume polyhedral shapes such that space is filled without voids while maintaining the uniform density dictated by short-range liquid-like packing of chain segments. Until recently, theory (*14*) and experiments (*15*) supported the notion that the universal equilibrium state is a bcc arrangement of such particles. Recent experiments with low molar mass (i.e., $N \approx 20$ to 100) 1,4-poly(isoprene)-*b*-poly(±-lactide) (PI-PLA) diblock copolymers (Fig. 1A) revealed the formation of the Frank-Kasper σ phase and the closely related dodecagonal quasicrystalline (DDQC) state when samples were cooled well below the order-disorder transition temperature (T_{ODT}), the equilibrium boundary between the ordered solid and disordered liquid phases (*16*–*18*). These observations, supported (in part) by self-consistent field theory (SCFT) (*19*), suggest enticing analogies between the underlying mechanisms responsible for symmetry-breaking in hard and soft matter. Accordingly, we have explored how thermal processing influences the nucleation and growth of order in asymmetric diblock copolymer melts based on the well-established effect of time and temperature on the formation of innumerable phases and microstructures in metal alloys.

Motivated by the wealth of documented metal-alloy Frank-Kasper phases (*20*) and a serendipitous discovery of the C14 phase with a short diblock copolymer (fig. S1), we used SCFT to establish whether other tetrahedral coordinated crystal structures might have competitive free energies at compositions where the σ phase occurs (*21*). An important ingredient in stabilizing the σ phase is conformational asymmetry, $b_A/b_B > 1$, where $b = R_g(6/N)^{1/2}$ is the statistical segment length and R_g is the unperturbed radius of gyration (*19*); $b_{PLA}/b_{PI} = 1.15$ (*22*, *23*). As shown in Fig. 1C and fig. S2, in addition to the previously computed A15 and σ phases (*19*), we have determined that conformationally asymmetric diblock copolymers can produce a host of other Frank-Kasper phases. These phases have free energies lying close to the lowest free-energy solution at intermediate segregation strength ($20 \le \chi N \le 40$) based on the mean-field analysis at compositions between bcc and hexagonally packed cylinders (HEX_C), where χ ($\sim T^{-1}$) is the Flory-Huggins segment-segment interaction parameter. (Here, we note that the magnitude of b_A/b_B required to generate these phases using the mean-field theory ($N \to \infty$) is considerably greater than b_{PLA}/b_{PI}, which we attribute to the finite length of the short PI and PLA blocks (*23*).) These results hint that many Frank-Kasper phases may be SCFT solutions.

All Frank-Kasper phases are formed by combining two, three, or four of the polyhedra (*20*) illustrated in planar graph form in Fig. 2A. These geometric objects contain pentagonal faces along with either no (Z_{12}), two (Z_{14}), three (Z_{15}), or four (Z_{16}) isolated hexagonal faces. The bcc structure contains only truncated dodecahedrons with square and hexagonal faces and is not classified as a Frank-Kasper phase. The SCFT calculations provide estimates for the relative volume, shape, and occupancy number for each type of polyhedron (table S2). Figure 2B illustrates the unit cells, polyhedron shapes, and distribution of micelles in four of the computationally stable crystal structures: bcc and the Frank-Kasper phases σ, C14, and C15. The σ phase has 30 particles per tetragonal unit cell drawn from Z_{12} (two shapes), Z_{14} (two shapes), and Z_{15} (one shape). Hexagonal C14 and cubic C15, common in many metal alloys such as $MgZn_2$ and Cu_2Mg, are often referred to as Laves phases (*3*). These crystal structures are formed from different combinations of Z_{12} and Z_{16}, with 12 and 24 particles per unit cell, respectively. Notably, the five, three, and two differently shaped polyhedra in σ, C14, and C15, respectively, have different volumes; hence, transformation between these and other states of organization in asymmetric block polymers requires mass (i.e., polymer chain) transfer.

These mean-field calculations ignore fluctuation effects, which strongly influence the structure

[1]Department of Chemical Engineering and Materials Science, University of Minnesota, Minneapolis, MN 55455-0132, USA. [2]Department of Chemistry, University of Minnesota, Minneapolis, MN 55455-0431, USA.
*These authors contributed equally to this work. †Present address: Materials Research Laboratory, University of California, Santa Barbara, CA 93106, USA. ‡Corresponding author. Email: dorfman@umn.edu (K.D.D.); bates001@umn.edu (F.S.B.)

of the disordered state when $\chi N < (\chi N)_{ODT}$ (*24*, *25*). Nevertheless, they suggest that the free-energy surface in the ordered regime at constant temperature presents numerous local minima that could be accessed by different melt processing strategies. Guided by these calculations, and inspired by the realization that many soft materials (e.g., proteins) are susceptible to process-path–driven metastable molecular configurations and morphologies (*26*), we subjected two PI-PLA diblock copolymer melts to two different thermal treatments. The polymers were synthesized using a well-established, two-step controlled polymerization procedure (*23*). Samples IL-58-15 (M_n = 5010 g/mol, $Đ$ = 1.08, f_L = 0.15) and IL-52-20 (M_n = 4830 g/mol, $Đ$ = 1.07, f_L = 0.20) were freeze-dried, hermetically sealed in aluminum pans, and then heated to a temperature several degrees above T_{ODT} = 99°C for IL-58-15 and above T_{ODT} = 132°C for IL-52-20. The block copolymers were then either (i) cooled directly to $T < T_{ODT}$ (at about 2°C/sec) or (ii) immediately submerged into liquid nitrogen (T = –196°C) then reheated to $T < T_{ODT}$ and held at the final target temperature for up to 20 days. Structural features were monitored using small-angle x-ray scattering (SAXS) measured at the Advanced Photon Source at Argonne National Laboratory.

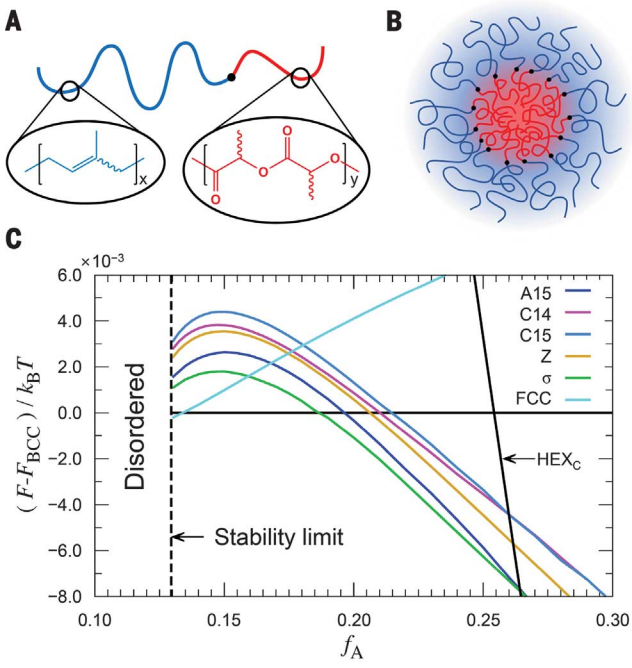

Fig. 1. SCFT free-energy calculation of asymmetric diblock copolymers. (**A** and **B**) Schematic representation of (A) AB diblock copolymer [(Inset) Chemical structures of PI and PLA blocks] and (B) a micelle particle formed by the polymer chains. (**C**) SCFT free-energy difference between various Frank-Kasper phases with respect to bcc as a function of f_A for χN = 40 and b_A/b_B = 2. See figs. S2 and S3 and table S1 for additional calculations.

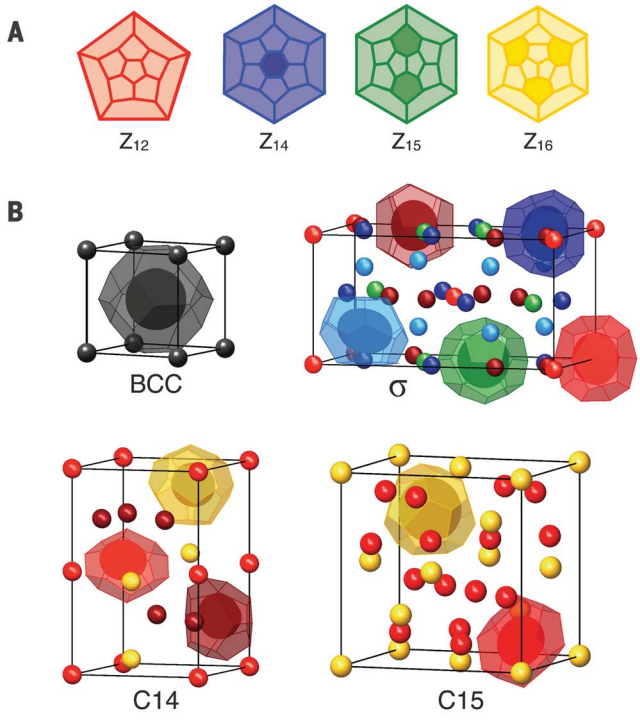

Fig. 2. Structural ingredients of the Frank-Kasper phases. (**A**) Planar graphs of the four polyhedra that combine to make Frank-Kasper phases. (**B**) Unit cells of bcc, σ, C14, and C15. The colors are correlated with the graphs in (A), where different particle shapes and volumes within a single type of polyhedron in σ and C14 are denoted by different hues. See figs. S4 to S7 for structural details of C14 and C15.

Figure 3 illustrates selected SAXS patterns recorded during various stages of the thermal processing applied to sample IL-58-15. At T = 105°C, the single broad scattering peak is consistent with an array of structured but disordered (DIS) micelles. Upon cooling to 70° and 55°C, the evolution of distinct diffraction patterns with time reveals the nucleation and growth of the bcc and the σ phases, respectively (*23*). This behavior is identical to what we reported for similar PI-PLA diblock copolymers (*16*–*18*). On the other hand, a sample that was rapidly quenched from DIS to –196°C and reheated to various temperatures below T_{ODT} resulted in several different states of order, depending on the final temperature. [The glass transition temperatures of the micelle corona ($T_{g,I}$ = –63°C) and core ($T_{g,L}$ = 8–14°C) blocks (fig. S8) are below all the targeted temperatures reported here.] At 25°C, the scattering pattern exhibits a broad peak and several weaker maxima that we associate with a state of kinetically arrested liquid-like packing (LLP), which we posit is reminiscent of the disordered phase structure. This type of soft glass occurs due to arrested molecular diffusion below the ergodicity temperature T_{erg} (*17*). With scarce mass exchange, the broad distribution of micelle volumes established in the disordered state is trapped, inhibiting the formation of discrete populations of micelle volumes associated with ordered phases. At 35°C, a SAXS pattern associated with the DDQC phase emerges after several days, whereas heating to 85°C produces a diffraction pattern consistent with the C14 phase (Fig. 3B and fig. S9).

Increasing f_L from 15 to 20%, at about the same molar mass, results in a different complement of ordered structures during thermal processing (Fig. 4). When cooled directly from DIS, sample IL-52-20 transforms rapidly to what we assign as HEX_C. We attribute the facile nature of this transition, which occurs as quickly as the specimen can be cooled (<1 min) even at $T_{ODT} - T$ = 80°C, to a different nucleation and growth mechanism; we speculate that this involves the fusion of micelles (*27*) and does not require diffusion of the core blocks through the corona matrix. Heating a quenched sample from –196° to 25°C again results in the LLP state, while the σ phase emerges at 85°C and a pattern consistent with the C15 phase (Fig. 4B and fig. S10) fully forms after several days at 100°C.

To a first approximation, packing of particles is controlled by the distribution of particle sizes. Nature provides a discrete set of atoms with individual radii that strongly influence the short-range length scales found in metal alloys driven by hard-core repulsion (*3*). The spatial arrangement of self-assembled diblock copolymer micelles also depends on short-range repulsive interactions. However, unlike individual atoms, each micelle

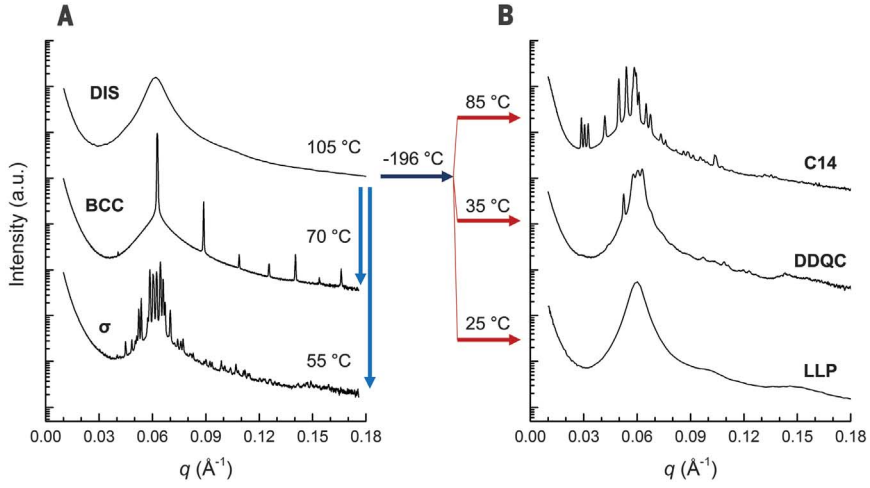

Fig. 3. SAXS patterns obtained from IL-58-15 after different thermal treatments. (**A**) Direct cooling from the disordered (DIS) state, where T_{ODT} = 99°C for the bcc to DIS transition, and (**B**) after immersion in liquid nitrogen and reheating. The data are vertically shifted for clarity.

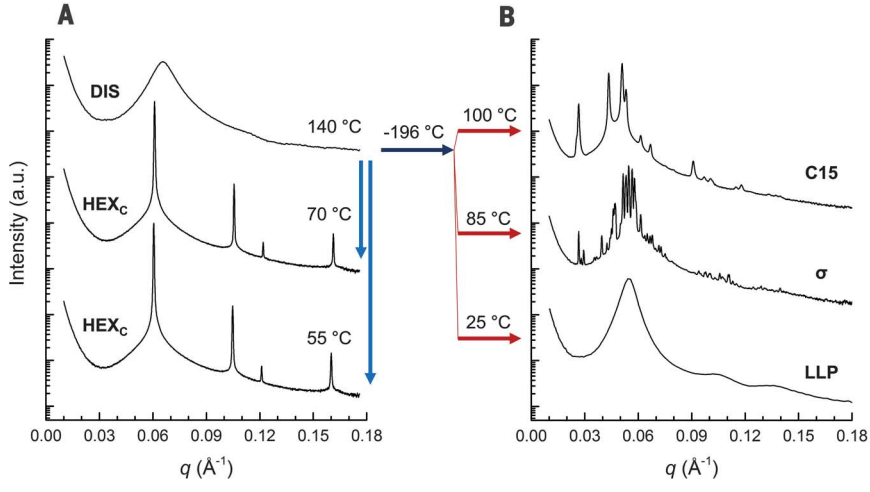

Fig. 4. SAXS patterns obtained from IL-52-20 after different thermal treatments. (**A** and **B**) Data were obtained using the same procedures identified in Fig. 3, where T_{ODT} = 132°C for the HEX_C to DIS transition. The data are vertically shifted for clarity.

can spontaneously adjust its size by shedding or absorbing diblock copolymer chains leading to a distribution of particle volumes; the observed disordered and ordered structures are formed by micelles containing 150 to 400 polymer chains. At equilibrium, the average particle diameter increases with decreasing temperature, $\langle D \rangle \sim \chi^{1/6}N^{2/3}$ (*11*); hence, rapidly supercooling the disordered melt to $T \ll T_{ODT}$ (e.g., by immersion in liquid nitrogen) drives the material far out of equilibrium. As the quenched material is heated above T_g, rearrangement of the particle sizes through fusion, fission, and chain diffusion stabilizes a state of local packing that guides nucleation and growth of long-range order along a path on the free-energy surface that apparently funnels into a local minimum associated with one of the low-symmetry phases. Once formed, free-energy barriers trap the various Frank-Kasper and quasicrystalline phases for long times. Cooling the disordered melt directly to temperatures where block copolymer diffusion remains rapid allows the system to continuously adjust the distribution of particle sizes, accessing an alternative path on the free-energy surface leading to the development of different states of order.

We and others have suggested that a geometric principle—denoted sphericity—influences the optimal array of particle sizes (*17*, *28*, *29*). Overall sphericity, calculated as the average isoperimetric quotient of the constituent polyhedra ($IQ = 36\pi V^2/S^3$, in which V and S are the particle volume and surface area, respectively; IQ = 1 for a sphere), is maximized by certain low-symmetry Frank-Kasper structures, where the ensemble average particle volume reflects a balance between minimizing chain-stretching (i.e., maximizing entropy) and minimizing the interfacial area between the core and corona blocks (i.e., minimizing enthalpy). Sphericity alone cannot explain the diversity of structures that emerge during the thermal processing of block polymers. Nevertheless, we note that all the Frank-Kasper phases we have considered in Fig. 1C have similar isoperimetric quotients (C14 and C15 are equal), notwithstanding the relatively diverse set of micelle volumes associated with the respective complement of polyhedra that make up each unit cell (table S2). We suspect that molar mass dispersity contributes to the rich assortment of phases described here, a feature recently shown by SCFT to stabilize the σ phase (*30*). In this regard, the shortness and unavoidable dispersity of the micelle core forming PLA blocks, just seven to nine number-average lactide repeat units, may be especially pertinent.

These results reinforce fundamental analogies between the way metals and self-assembled soft materials break symmetry when subjected to changes in thermodynamic state variables that drive phase transitions. Competition between lattice symmetry and the drive to minimize system free energy through tailoring of the overall size and shape of the polyhedral micelles in real space has intriguing analogies with the competition between the packing of metal atoms, where the tendency for the electronic configuration to support a nearly spherical Fermi surface can induce transitions to low-symmetry reciprocal space lattices (*17*, *31*, *32*). The exquisite control over block polymer molecular structure afforded by controlled polymerization offers opportunities to unravel the basic principles that define order and disorder in condensed matter.

REFERENCES AND NOTES

1. D. Hobbs, J. Hafner, D. Spišák, *Phys. Rev. B* **68**, 014407 (2003).
2. S. S. Hecker, *Los Alamos Sci.* **26**, 290–335 (2000).
3. M. De Graef, M. E. McHenry, *Structure of Materials: An Introduction to Crystallography, Diffraction and Symmetry* (Cambridge Univ. Press, New York, ed. 2, 2012).
4. D. Shechtman, I. Blech, D. Gratias, J. W. Cahn, *Phys. Rev. Lett.* **53**, 1951–1953 (1984).
5. F. C. Frank, J. S. Kasper, *Acta Crystallogr.* **12**, 483–499 (1959).
6. R. F. Berger, P. L. Walters, S. Lee, R. Hoffmann, *Chem. Rev.* **111**, 4522–4545 (2011).
7. J. M. Seddon, J. Robins, T. Gulik-Krzywicki, H. Delacroix, *Phys. Chem. Chem. Phys.* **2**, 4485–4493 (2000).
8. G. Ungar, Y. Liu, X. Zeng, V. Percec, W.-D. Cho, *Science* **299**, 1208–1211 (2003).
9. G. Ungar, X. Zeng, *Soft Matter* **1**, 95–106 (2005).
10. M. Huang *et al.*, *Science* **348**, 424–428 (2015).
11. F. S. Bates, G. H. Fredrickson, *Phys. Today* **52**, 32–38 (1999).
12. F. S. Bates *et al.*, *Science* **336**, 434–440 (2012).
13. F. S. Bates, G. H. Fredrickson, *Annu. Rev. Phys. Chem.* **41**, 525–557 (1990).
14. L. Leibler, *Macromolecules* **13**, 1602–1617 (1980).
15. C. D. Han *et al.*, *Macromolecules* **33**, 3767–3780 (2000).
16. S. Lee, M. J. Bluemle, F. S. Bates, *Science* **330**, 349–353 (2010).
17. S. Lee, C. Leighton, F. S. Bates, *Proc. Natl. Acad. Sci. U.S.A.* **111**, 17723–17731 (2014).
18. T. M. Gillard, S. Lee, F. S. Bates, *Proc. Natl. Acad. Sci. U.S.A.* **113**, 5167–5172 (2016).
19. N. Xie, W. Li, F. Qiu, A.-C. Shi, *ACS Macro Lett.* **3**, 906–910 (2014).
20. M. Dutour Sikirić, O. Delgado-Friedrichs, M. Deza, *Acta Crystallogr. A* **66**, 602–615 (2010).
21. A. Arora *et al.*, *Macromolecules* **49**, 4675–4690 (2016).
22. S. Lee, T. M. Gillard, F. S. Bates, *AIChE J.* **59**, 3502–3513 (2013).
23. See the supplementary materials.

24. G. H. Fredrickson, E. Helfand, *J. Chem. Phys.* **87**, 697–705 (1987).
25. P. Medapuram, J. Glaser, D. C. Morse, *Macromolecules* **48**, 819–839 (2015).
26. M. Karplus, J. A. McCammon, *Nat. Struct. Biol.* **9**, 646–652 (2002).
27. K. A. Koppi, M. Tirrell, F. S. Bates, K. Almdal, K. Mortensen, *J. Rheol.* **38**, 999–1027 (1994).
28. M. Rappolt, F. Cacho-Nerin, C. Morello, A. Yaghmur, *Soft Matter* **9**, 6291–6300 (2013).
29. G. M. Grason, B. A. DiDonna, R. D. Kamien, *Phys. Rev. Lett.* **91**, 058304 (2003).
30. M. Liu, Y. Qiang, W. Li, F. Qiu, A.-C. Shi, *ACS Macro Lett.* **5**, 1167–1171 (2016).
31. S. Lee *et al.*, *Chem. Eur. J.* **19**, 10244–10270 (2013).
32. R. Lifshitz, *Proc. Natl. Acad. Sci. U.S.A.* **111**, 17698–17699 (2014).

ACKNOWLEDGMENTS

This work was supported by the National Science Foundation under grants DMR-1104368 and DMR-1333669. Use of the Advanced Photon Source (APS) at Argonne National Laboratory was supported by the U.S. Department of Energy, Office of Science, under contract DE-AC02-06CH11357. Portions were performed at the DuPont-Northwestern-Dow Collaborative Access Team (DND-CAT) located at Sector 5 of the APS, supported by E. I. DuPont de Nemours and Co., The Dow Chemical Company, and Northwestern University. K.K. and F.S.B. designed the research on PI-PLA. K.K. synthesized the PI-PLA samples and acquired and analyzed SAXS data. M.W.S., R.M.L., and M.A.H. designed the research on poly(ethylethylene)-*b*-poly(±)-lactide (PEE-PLA). M.W.S. and R.M.L. synthesized the PEE-PLA samples and performed SAXS experiments. M.W.S. conceived of and demonstrated the liquid nitrogen thermal processing technique with the PEE-PLA and initially identified the C14 phase. A.A. and K.D.D. designed, executed, and interpreted SCFT calculations. F.S.B. supervised the overall project and drafted the initial manuscript. All authors reviewed and edited the manuscript and supplementary materials.

SUPPLEMENTARY MATERIALS

www.sciencemag.org/content/356/6337/520/suppl/DC1
Materials and Methods
Figs. S1 to S15
Tables S1 to S5
References (*33*–*44*)

6 January 2017; accepted 8 March 2017
10.1126/science.aam7212

Thermal processing of diblock copolymer melts mimics metallurgy

Kyungtae Kim, Morgan W. Schulze, Akash Arora, Ronald M. Lewis III, Marc A. Hillmyer, Kevin D. Dorfman and Frank S. Bates

Science **356** (6337), 520-523.
DOI: 10.1126/science.aam7212

When polymers behave like metals

Diblock copolymers, in which two dissimilar chains are chemically linked, can show a rich array of morphologies. These are usually attained by slow cooling to give the chains time to find their thermodynamically preferred arrangements. Rather than using slow cooling, Kim *et al.* rapidly quenched their materials from the disordered state and then annealed at low to moderate temperatures (see the Perspective by Stein). Different processing routes drove assembly into a variety of low-dimensional phases more typical of metal alloys.

Science, this issue p. 520; see also p. 487